Formation of nick instabilities due to particle clustering along crystal interfaces

N. Vandewalle,[1,*] M. Ausloos,[1] and R. Cloots[2]
[1]*SUPRAS, Institut de Physique B5, Université de Liège, Sart Tilman, B-4000 Liège, Belgium*
[2]*SUPRAS, Institut de Chimie B6, Université de Liège, Sart Tilman, B-4000 Liège, Belgium*
(Received 10 March 1997)

The kinetic growth of crystal grains is simulated on a square lattice in the presence of mobile particles. The model is based on the Eden and the dynamic epidemic models. Trapping of the particles by the advancing front and a short-range repulsion of the particles by the front are both allowed. The grain boundary morphology is studied through the kink density concept and the spatial distribution of particles is discussed. Indeed, the clustering of particles along the crystal edges is found to induce the formation of so-called nick instabilities at the liquid-solid interface. The particles, when trapped near such instabilities, occur as oblique filamentary structures in the crystal matrix, just like river networks. These findings agree with recent experimental observations. The numerical laws are also explained by theoretical arguments based on different characteristic lengths. [S1063-651X(97)08810-7]

PACS number(s): 05.40.+j, 81.10.Aj

I. INTRODUCTION

The interaction between some mesoscopic particles and an advancing solid-liquid front is of fundamental interest in various fields of science. Indeed, numerous systems are related to such a problem, e.g., the behavior of biological cells on an ice-water interface [1], the trapping of bubbles during solidification [2], or the growth of superconducting $YBa_2Cu_3O_{7-x}/Y_2BaCuO_5$ composites [3]. In the particular field of crystal growth, it is of interest to consider the trapping problem of particles in order to control the decoration of a crystal by mesoscopic impurities. Indeed, trapped impurities control the microstructural features and the physical properties of the materials as for the particular case of $YBa_2Cu_3O_{7-x}$ [4]. From the statistical physics point of view, it is of interest to study how the interface shape is affected by the presence of a collection of particles.

The trapping or pushing of a mesoscopic impurity by an advancing solid front through a liquid has been discussed by Uhlmann, Chalmers, and Jackson [5]. They experimentally studied the growth of a planar solid-liquid interface reaching a *single* perfectly smooth particle. They observed that for typical growth conditions, there exists a critical particle radius R_c above which the particle is trapped by the front and below which the particle remains indefinitely pushed by the growing front. In a Uhlmann-Chalmers-Jackson (UCJ) process, the value of R_c depends on physical parameters such as the nature of the medium, the nature of the particle, the velocity of the front, the viscosity of the liquid phase, and the microscopic roughness of the particle. A practical criterion [1] in crystal growth is that the pushing-trapping phenomenology is usually expected to take place for the product $R_c v$ around 10^{-6} cm^2/s. Thus the pushing-trapping transition occurs typically at the mesoscopic scale for crystal growth.

Recently, we have introduced a simple model, the so-called dynamic epidemic model [6,7], which considers a meandering interface pushing a collection of smooth mobile particles. It has been shown that this process leads to the aggregation of particles along the front and further leads to a nontrivial trapping of the aggregates. This effect has been related [7] to a percolationlike transition occurring as a function of the particle fraction.

In the present work we consider the case for which a smooth front (like a solidification front), instead of a rough interface as considered in our previous works, reaches a collection of particles. Moreover, we consider the case of low particle fractions, i.e., far from a percolation transition. This is much more relevant for fulfilling crystal growth conditions. We investigate such a situation through a combination of the so-called dynamic epidemic model [7] and an extended Eden model [8]. We discuss the final spatial distribution and the grain morphology and give theoretical arguments to explain the observations.

II. MODEL

We consider a two-dimensional square lattice. The model is mesoscopic in the sense that each site can receive either a solid (S) crystal ''unit,'' a liquid (L) unit, or a particle (P). Liquid units, solid units, and particles are represented, respectively, on each site i by the variables $c_L(i)$, $c_S(i)$, and $c_P(i)$, taking only the integer value 1 or 0 for the presence or absence of the phase on this site. Because a site i can only contain a single phase, the relation $c_L(i)+c_S(i)+c_P(i)=1$ is implied. Initially, all sites contain the liquid phase, except an *a priori* fraction x of sites that are filled with a particle. Thus the average of $c_P(i)$ over all lattice sites gives trivially $\langle c_P \rangle = x$.

The single-grain growth process starts with an inner (central) site turning into the solid phase; this site becomes the nucleus of the grain growth. The grain growth then follows an Eden growth process adapted to crystal growth [9] as follows. Each step of the growth process consists in selecting all unoccupied (liquid) sites j in contact with the growing cluster (solid). A growth probability weight P_j is associated with each selected site j. This weight constraint is first imposed in order to take anisotropic crystal growth rates into

*Electronic address: vandewal@gw.unipc.ulg.ac.be

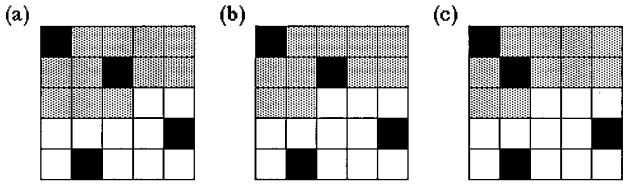

FIG. 1. Schematic illustration of one growth step on a small part of the front. The particle, liquid, and crystal phases are represented in black, gray, and white, respectively: (a) a central site that is a kink site is chosen for the growth step; (b) in this site the liquid phase is turned into the crystal phase; (c) the particle touched by the growth front makes a move decreasing its contact with the front.

account as in Ref. [9]. The growth probability P_j on one of the possible j growth sites is assumed to be proportional to

$$P_j \sim \exp\left[g_{\mathrm{NN}} \sum_m c_S(m) \right], \tag{1}$$

where the summations run over all the nearest-neighbor (NN) m sites of the selected j site. The exponential form (Boltzmann-like) of Eq. (1) is used to enhance the bonding anisotropy along $\langle 10 \rangle$ and $\langle 01 \rangle$ lattice directions and to mimic an activation energy process [9]. The parameter g_{NN} is like the bond energy in the lattice-gas model. It is a dimensionless parameter. It can be argued [9] that g_{NN} has the simple form $g_{\mathrm{NN}} = J_{\mathrm{NN}}/k_B \Delta T$, where J_{NN} is a coupling energy, k_B is the Boltzmann constant, and ΔT is the departure from the equilibrium temperature (undercooling). The probabilities P_j are stored in an array, renormalized over the interval [0,1], and a specific growth site is chosen by randomly. The solidification of the mesoscopic cell is then supposed to take place there.

As an example, a small part of the front is shown at three consecutive time steps in Fig. 1, where the crystal phase is drawn in white, the liquid phase in gray, and the particles in black. In Fig. 1(a) the central liquid site was chosen to turn into the solid phase [see Fig. 1(b)].

After each growth step that results in gluing a new crystal unit on the front, the untrapped particles that are in contact with the new crystal unit are selected. Each selected particle is either assumed to be blocked and to become trapped for ever by the crystal with a probability p, or a dynamical UCJ-like event is allowed to take place with a probability $1-p$. One should note that the UCJ theory considers only the two extreme cases $p=0$ and 1 for particle radii $R<R_c$ and $R>R_c$, respectively. In real situations, the size of the particles may be polydisperse. The roughness of the particle may be also considered to be different from one particle to another. Thus a noninteger probability p allows one to consider that the particles are not identical. We are of course aware that a true process cannot be represented by a single number.

For a UCJ event, the number of nearest-neighbor solid units of the particle has to be calculated. This is called the contact number of the particle. The contact number of the neighboring empty (liquid) sites is also calculated. If one (or more) neighboring site(s) has (have) a contact number strictly less than the contact number of the particle itself, the latter makes a random jump towards one such site in order to reduce its contact number. In Fig. 1(b), for example, we let the particle that is touched by the front to be subjected to an UCJ event and thus be allowed to make a jump towards a nearest-neighbor site [as drawn in Fig. 1(c)].

Notice that if no low contact number is available on a nearest-neighbor liquid site, the particle cannot make any move, although a UCJ event is allowed. This is another way for a particle to be trapped. A new growth step is then taken. The whole process described in the previous paragraphs is repeated a desired number N of times.

It is useful to discuss the physical range of validity of the model and stress it with respect to the mesoscopic scale. Rearrangements on a crystal surface are essentially evaporation-diffusion processes occurring at the microscopic level. The model does not need to include such diffusion processes. Indeed, the ensemble average will take care of such fine features occurring at a different time scale. The strict validity condition imposes that the mesoscopic cells considered by the model should thus be larger than the diffusion length of atoms in the melt. Consider that the diffusion length $\lambda = \sqrt{D\tau}$, with a characteristic time interval τ as, e.g., the time to grow the solid phase on a cell. This characteristic time τ is simply $\tau = a/v$, where a is the size of a lattice mesoscopic cell of the model and v the growth rate of the solid phase. The above model is thus valid if $\lambda < a$, i.e.,

$$D/v < a. \tag{2}$$

Thus the model should consider a ''sufficient large scale'' depending on the physical quantities presented by the physical situation. Typically, the unit size a should be a mesoscopic length, i.e., the size of the considered impurities. For instance, for the $YBa_2Cu_3O_{7-x}$, system cited in the Introduction, the diffusion coefficient D is about 10^{-11} m^2/s [10] and the usual growth rate v is of the order of 1 mm/h [10]. Thus the condition (2) is verified if a is larger than 1 μm. This size is roughly the size of the Y_2BaCuO_5 particles, i.e., the minimum scale of the mesoscopic microstructure of interest. Application of the above model to $YBa_2Cu_3O_{7-x}$ ceramics can be found in Ref. [11].

III. NUMERICAL RESULTS

Let us recall that a growing site is defined as a site containing the liquid phase and being a nearest neighbor of a crystal unit. A kink site is defined as a growing site (liquid) having strictly more than one crystal neighboring units. For example, the site chosen for growth in Fig. 1(a) was a kink site. The kink sites are also ''hot sites'' since they are most probably chosen during the crystal growth [see Eq. (2)].

We define and introduce the notion of the kink site density k as the ratio between the number of kink sites and the total number of possible growing sites at each time step. A crystal with ''perfect'' smooth edges along the $\langle 10 \rangle$ and $\langle 01 \rangle$ directions has $k=0$. As the crystal grows, the kink site density k is numerically found to fluctuate around a value depending on g_{NN} [9]. A recent work [12] has shown that the kink density depends exponentially on g_{NN}. The higher the g_{NN}, the lower the kink site density k.

In the present study, g_{NN} was arbitrary fixed to be 200, a value that gives smooth edges in the absence of particles [9]. This value is reasonable as a relative value of the ratio be-

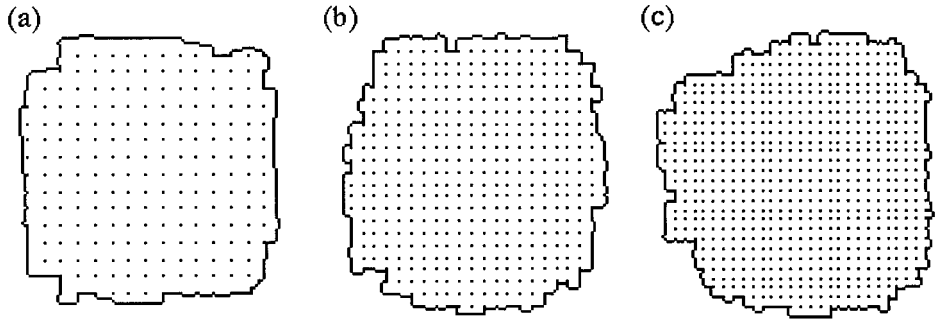

FIG. 2. Typical boundaries for grains made of $N=10\,000$ crystal units. The trapped particles are also shown. The particles are static ($p=1$). Three different concentrations of particles are illustrated: (a) $x=\frac{1}{49}$, (b) $x=\frac{1}{25}$, and (c) $x=\frac{1}{16}$.

tween the bond energy and the out-of-equilibrium temperature range as mentioned above. In this section we study the effect of the other parameters (x and p) on the global crystal shape, on the local surface morphology (through k), and on the spatial distribution of trapped particles.

In the simulations reported here, the initial distribution of particles was often chosen to be spatially regular rather than random in order to have initially disconnected particles and in order to emphasize the displacement of particles through the UCJ mechanism. At the beginning of the simulation, the particles were separated by a fixed integer distance d along both $\langle 10\rangle$ and $\langle 01\rangle$ directions such that the x concentration value is given by $1/d^2$. The results, however, were found to be similar for random or regular particle distributions.

Let us examine first the case for which the trapping probability has the maximum value ($p=1$) such that the particles represent static hindrances for the growing front. The resulting crystal shape and the trapped particles are shown in Fig. 2 for different x concentrations: (a) $x=\frac{1}{49}$,(b) $x=\frac{1}{25}$, and (c) $x=\frac{1}{16}$. Each grain is made of $N=10\,000$ crystal units. For a large concentration x, the front is jagged since the particles greatly perturb the front. The grain shape becomes less squarelike as the fraction x is increased [see Fig. 2(c)].

Figure 3 presents in a semilogarithmic plot the kink site density k of such $N=10\,000$ grains as a function of the square root of the concentration x. The parameter p is fixed to be $p=1$, as in Figs. 2(a)–2(c). Each dot represents an average of k over 20 simulated grains. Circles and triangles are used for random or regular initial particle distributions, respectively. No significative change of k is observed between the random and the regular initial particle distributions. One should note that the values of the kink site density is low (of the order of 10^{-1}) because of the high value of g_{NN} [9]. For both random and regular initial particle distributions, a decrease of k is observed as the amount of particles is increased. In the presence of particles, the number of growing sites decreases because particles ''infect'' the surface. The results of Fig. 3 show that the kink site density k decreases also with x, a result that was unexpected by a comparison with Fig. 2. Therefore, we emphasize that a low kink site density does not correspond necessarily to smooth edges and to a square symmetry. On a length scale less than the particle interdistance, the edges are flat even though the global shape looks rounded [see Fig. 2(c)].

For a periodic initial particle distribution and for $p=1$, i.e., static particles, the maximum x fraction allowing for an infinite growth is obviously $x=\frac{1}{4}$ with a minimum particle interdistance $d=2$. However, for a random initial particle distribution, the maximum fraction of particles allowing the growth is about $x_c\approx 0.41$ for $p=1$. This critical value x_c corresponds to the random-site percolation threshold [13] on the square lattice for the fraction of initial liquid site $1-x_c\approx 0.59$. For $p=0$, a previous work [6] has shown that the transition occurs at $x_c=0.56\pm 0.01$, i.e., at a quite larger fraction of particles.

For the investigated values of x and $p=1$, the decrease of the kink site density k is empirically found to be a stretched exponential

$$k_{(p=1)}\sim \exp(-\gamma\sqrt{x}), \tag{3}$$

for $x<x_c$, the amplitude of the stretched exponential depending on the size of the grain. The continuous curve of Fig. 3 is a fit of the data with the latter equation giving $\gamma\approx 5.745$.

It is of interest to examine the effect of p on the grain shape. Figures 4(a)–4(c) present three grains that are growing with different trapping probabilities p. Each grain is made of $N=10\,000$ crystal units and the concentration x is

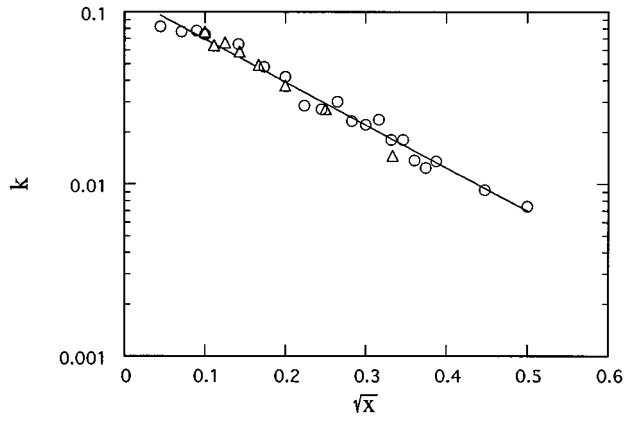

FIG. 3. Kink site density k as a function of the square root of the particle concentration x for $N=10\,000$ grains. The particles are static ($p=1$). Each dot is an average over 20 simulations. The circles and triangles represent the use of random or regular initial particle distributions, respectively. The continuous line is a fit with the stretched exponential of Eq. (3).

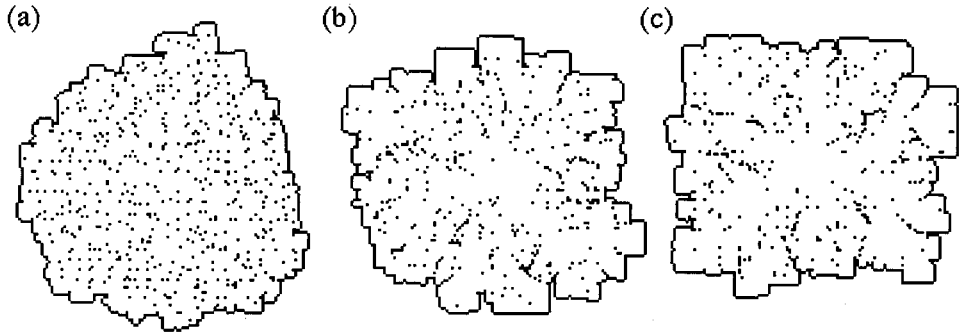

FIG. 4. Grain boundaries and trapped particles shown for three grains made of $N=10\,000$ crystal units. The concentration of particles is set to $x=\frac{1}{16}$. Three different values of the trapping probability are illustrated: (a) $p=0.16$, (b) $p=0.04$, and (c) $p=0.01$.

kept constant ($x=\frac{1}{16}$). For large-p values [Fig. 4(a), the grain internal particle distribution is perturbed, but is still homogeneous, as was the initial particle distribution. When decreasing the trapping probability p, flat edges locally appear together with particle-free regions [Fig. 4(b)]. However, the particles aggregate on the edges of the grain [Fig. 4(c)]. The accumulation of particles locally leads to the formation of ''nicks'' on the growth front. This mechanism results also in the trapping of aggregates in the crystal matrix. Large inhomogeneities and clusters of particles behind nicks are clearly seen in Fig. 4(c). These inhomogeneities look like filaments. The trapping events seem to be a cooperative phenomenon for low trapping probabilities.

Figure 5 presents on a semilogarithmic plot the kink site density k as a function of the particle fraction x and for *non–a priori* trapping situation ($p=0$). Each dot represents an average over 20 simulated grains of size $N=10\,000$. The kink site density k decreases as the fraction x increases. This seems similar to what was observed above for the $p=1$ case (see Fig. 3). However, the kink site density is found to be a simple (nonstretched) exponential

$$k_{(p=0)}\sim\exp(-\gamma x) \tag{4}$$

for $x<x_c$, the amplitude of the exponential depending on the grain size N. The continuous curve in Fig. 5 is a fit with Eq. (4), giving $\gamma\approx 10.962$.

IV. DISCUSSION

In this section we consider the kinetic mechanisms and interpret the numerical results on the kink site density k. The parameters g_{NN}, p, and x of the model constitute the basic relevant set because the tuning of each parameter separately induces both globally and locally different morphological changes as experimentally observed. A wide variety of observed kinetic behaviors and morphologies can be produced by the present model. The most interesting result is the observation of inhomogeneous nontrivial particle distributions obtained even for low trapping probabilities.

We recall that two sorts of trapping mechanisms can take place on the advancing front: (i) the particles in contact with the front are trapped with a probability p or (ii) the clustering of particles (for $p\rightarrow 0$) ahead of the front obstructs the displacement of some of them and leads to their trapping by the front. For both types of trapping events, the flat front is perturbed and the relaxation of the front towards a new flat configuration depends on the parameter strengths.

For high-p values ($p\approx 1$), the particles are of course easily trapped and the accumulation of particles on the growing front cannot occur. Particles alone represent small hindrances for the front. The front is deformed by the presence of such particles [see Fig. 2(c)]. The front is rough on a scale larger than the particle interdistance δ_{part}. In general, one particle occupies a site having more than one nearest-neighbor crystal unit. In other words, the interface is pinned by the static particles. This is schematically drawn in Fig. 6(a). Those sites are candidates to be kink sites, but are removed from the number of possible growth sites. This explains why the kink site density k decreases with x. In fact, the edges of the crystal remains flat, but only on length scales corresponding to the particle interdistance δ_{part}. Because the kink sites tend to be occupied by a particle, the distance between two kink sites δ_{kink} is proportional to $\exp(\delta_{\mathrm{part}})$, i.e., the exponential of the particle interdistance. Since on average $\delta_{\mathrm{part}}\sim 1/\sqrt{x}$ for static particles and somewhat by definition $1/\delta_{\mathrm{kink}}\approx k$, one recovers the results of Fig. 3 and the stretched exponential for k [Eq. (3)].

For low trapping events ($p\approx 0$), the particles move along the front, resulting in a local accumulation of the particles on the front [Fig. 6(b)]. Such clusters obstruct the advancing

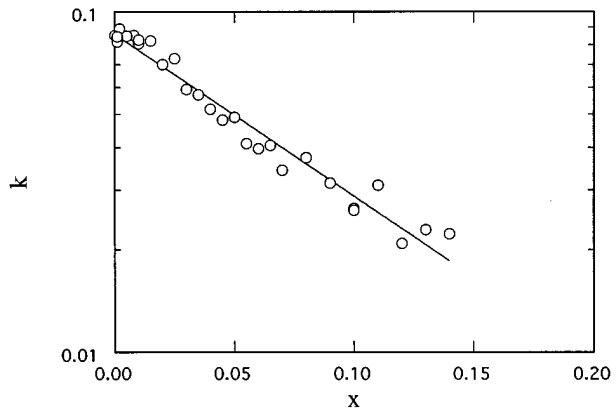

FIG. 5. Semilogarithmic plot of the kink site density k as a function of the particle fraction x for $N=10\,000$ grains. The particles are pushed by the interface ($p=0$). Each dot represents an average over 20 simulations. The continuous line is a fit with the simple exponential law of Eq. (4).

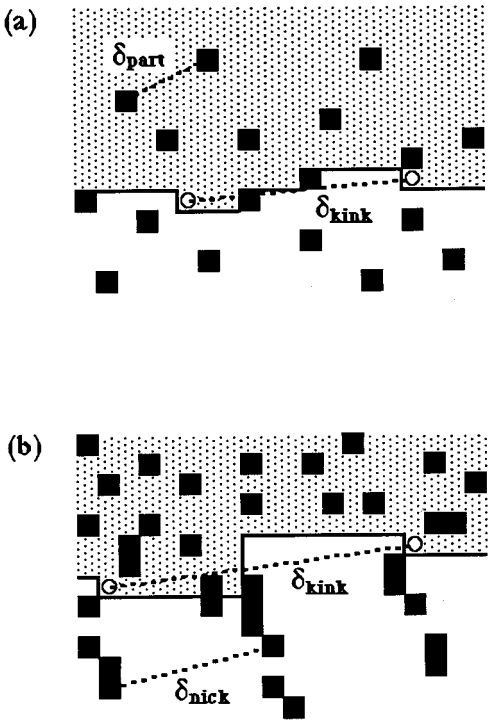

FIG. 6. Schematic illustrations of the typical interface morphology for two different situations: (a) the particles are static ($p=1$) and (b) the particles are pushed by the interface ($p=0$) leading to the formation of nicks and filaments. The particle, liquid, and crystal phases are represented in black, gray, and white, respectively. The different length scales discussed in the text are emphasized.

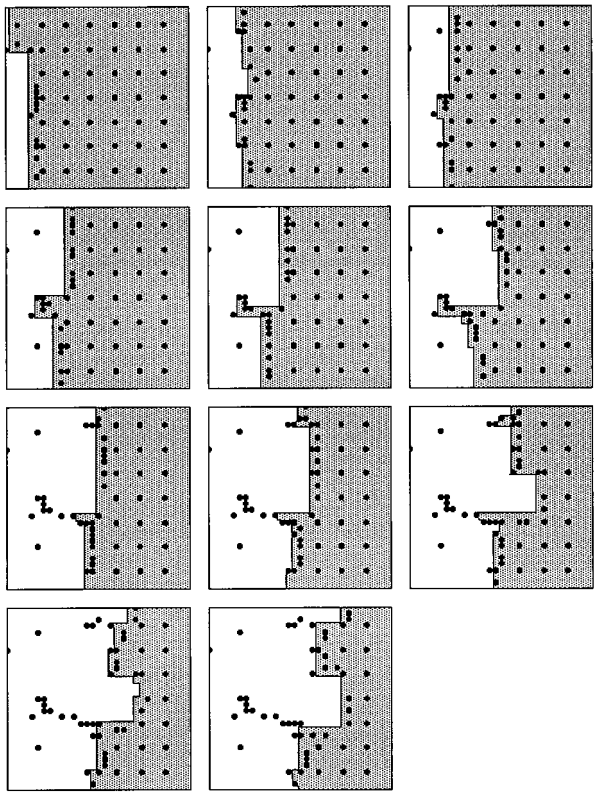

FIG. 7. Different time steps in the formation of a nick on the edge due to the accumulation and trapping of particles. The time steps evolve from left to right and from top to bottom.

front and a nick is created. Figure 7 presents different time steps of the typical formation of such a nick. Trapped and untrapped particles are drawn. The structure of trapped particles looks like ''filaments.'' These trapped structures were recently observed in KCl crystals decorated by SiO_2-Al_2O_3 particles [14]. Filamentary structures of trapped particles have been observed also in the directional solidification of reinforced aluminium based materials [15]. Finally, the UCJ mechanism has been shown recently to describe the occurrence of filamentary structures in $YBa_2Cu_3O_{7-x}$ superconducting ceramics [16].

An interesting result is that a nick cannot easily disappear for high-x values because additional particles fall into the nick as the front advances. Moreover, the motion of nicks results in some sort of drag, thus in filaments growing sideways to the main growth directions. For very-high-x values, we observe the collapse of two or several nicks. This results in the formation of treelike structures or ''river network–like'' structures. Such a structure is illustrated in Fig. 8 for a grain of $N=20\,000$ crystal units growing in the presence of a high density of particles ($x=\frac{1}{9}$ and $p=0.01$). For $p\rightarrow 0$, the edges of the grain remain flat, but only on length scales corresponding to the nick interdistance δ_{nick}, i.e., $\delta_{\mathrm{kink}} \sim \exp(\delta_{\mathrm{nick}})$. Due to the filamentary structures of particles trapped behind the nicks, one would expect that $\delta_{\mathrm{nick}} \sim 1/x$ such that one recovers the results of Fig. 3 and the simple nonstretched exponential of Eq. (4).

V. CONCLUSION

From the kinetic growth simulation of two-dimensional grains taking into account the presence of mesoscopic particles either trapped or pushed by the interface, the local and global crystal morphologies as well as the trapped spatial distribution have been studied and discussed. The UCJ-like mechanism is found to induce the formation of the so-called nick instabilities on the edges of the crystal. The particles,

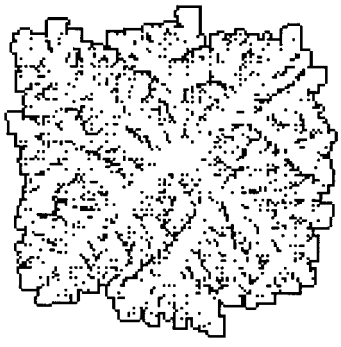

FIG. 8. Grain of $N=20\,000$ crystal units. The distribution of trapped particles is also shown and is seen to lead to different features in particular filaments going sideways and ''river networks.'' The grain has been grown in the presence of a high concentration of particles ($x=\frac{1}{9}$). The UCJ mechanism has been enhanced by taking $p=0.01$.

which are trapped around such instabilities, lead to the formation of filamentary structures (or patterns) in the crystal matrix. The density of kinks is a nontrivial function of the concentration of mobile particles and the strength of the front-particle interaction. This agrees with recent experimental observations on layerlike systems with strong growth anisotropy. The three-dimensional cases should motivate some interesting work in the future. Moreover, the river network structure could be quantified in further work both at the simulation and at the experimental stages.

ACKNOWLEDGMENTS

Part of this work was supported through the Minister of Education under Contract No. ARC (94-99/174) of ULg. A special grant from FNRS/LOTTO allowed us to perform specific numerical work.

[1] C. Körber, Q. Rev. Biophys. **21**, 229 (1988).
[2] T. O. D. Hanley and T. Vo Van, J. Cryst. Growth **19**, 147 (1973).
[3] C.-J. Kim, S. H. Lai, and P. J. McGinn, Mater. Lett. **19**, 185 (1994); N. Vandewalle, M. Ausloos, N. Mineur, R. Cloots, G.-W. Hong, and C.-J. Kim, Supercond. Sci. Technol. **9**, 665 (1996).
[4] F. Sandiumenge, S. Piñol, X. Obradors, E. Snoeck, and C. Roucau, Phys. Rev. B **50**, 7032 (1994).
[5] D. R. Uhlmann, B. Chalmers, and K. A. Jackson, J. Appl. Phys. **35**, 2986 (1964).
[6] N. Vandewalle and M. Ausloos, J. Phys. A **29**, 309 (1996).
[7] N. Vandewalle and M. Ausloos, Phys. Rev. Lett. **77**, 510 (1996).
[8] M. Eden, in *Symposium on Information Theory in Biology*, edited by H. P. Yockey (Pergamon, New York, 1958), p. 359; R. Jullien and R. Botet, J. Phys. A **18**, 2279 (1985).
[9] N. Vandewalle, M. Ausloos, and R. Cloots, Philos. Mag. A **72**, 727 (1995).
[10] S. P. Athur, V. Selvamanickam, U. Balachandran, and K. Salama, J. Mater. Res. **11**, 2976 (1996).
[11] N. Vandewalle, R. Cloots, and M. Ausloos, Supercond. Sci. Technol. **10**, 123 (1997).
[12] M. Kotrla (private communication) has shown that $k \sim \exp(-g_{nn})$; see also M. Kotrla and M. Predota, Europhys. Lett. **39**, 251 (1997).
[13] D. Stauffer and A. Aharony, *Introduction to Percolation Theory* (Taylor & Francis, London, 1992).
[14] N. Vandewalle, Ph.D. thesis, University of Liège, 1996 (unpublished).
[15] U. Hecht and S. Rex, Metall. Mater. Trans. A **28**, 867 (1997).
[16] C. Varanasi, M. A. Black, and P. J. McGinn, J. Mater. Res. **11**, 565 (1996).